journal

J. Am. Ceram. Soc., 86 [12] 2087–92 (2003)

Determination of the Minimum Time for Binder Removal and Optimum Geometry for Three-Dimensional Porous Green Bodies

Stephen J. Lombardo*,†

Department of Chemical Engineering, University of Missouri, Columbia, Missouri 65211

Z. C. Feng

Department of Mechanical and Aerospace Engineering, University of Missouri, Columbia, Missouri 65211

A model is developed to optimize two aspects of the thermal removal of binder from green ceramic components. The model, which accounts for flow in porous media arising from the thermal decomposition of binder in three-dimensional bodies with anisotropic permeability, describes the pressure within the body as a function of position, time, and temperature during the heating cycle. The model is used with variational calculus to predict the heating profile that minimizes the cycle time for the thermal removal of binder. The model is also used to determine which body geometry maximizes the buildup of pressure in parallelepipeds, a common shape of multilayer ceramic capacitors.

I. Introduction

During thermolysis of binder[1–8] from ceramic bodies moderately loaded with polymer, for which open porosity exists, failure of the component is often attributed to stresses arising from the buildup of pressure within the pore space. The internal pressure varies as the binder decomposes and the gas-phase degradation products exit the body under the influence of a pressure gradient. We have recently examined the relationship between stresses and pressures during binder removal from three-dimensional porous shapes.[9,10] In the formulation of the stress problem, the gradient in pressure within the green body appears as an internal body force. To be able to include the pressure distribution in the finite element simulations for predicting the stress, we have developed an approximate analytical solution for the pressure distribution and have recently shown that this is very accurate when compared with the numerical results.[11] As an outcome of this analysis, we have shown that the maxima in pressure and normal stresses appear in the center of the body and that they are proportional to each other. The shear stresses which occur are typically an order of magnitude lower and do not appear in the body center.

Because the maximum normal stresses and the maximum pressure are proportional, and because we have an analytical solution for the latter, we can use the model for the pressure distribution to develop relationships between pressure buildup, body geometry, and the cycle time for binder removal.[12–14] In this work, we first present the three-dimensional model for describing pressure-driven flow in porous media when a source term is present. We next show how the minimum cycle time for binder removal can be established by using calculus of variations. Although we have already developed this formalism for one-dimensional bodies,[12] we are now able to extend the algorithm to three-dimensional shapes.

Finally, we indicate how the model for describing the pressure distribution can be used to design the shape of multilayer ceramic capacitors to mitigate the buildup of pressure during binder removal cycles. This becomes important as capacitor size increases for increased charge storage. An important feature of the model for predicting the pressure distribution is that it can treat anisotropic permeability within the body, which has been observed in multilayer ceramic capacitors where the flow is preferential in the direction parallel to the metal electrode layers.[13]

II. Model

The model treats flow in porous green bodies arising from the pressure gradients which occur from the decomposition products of thermal binder degradation. The model has been derived in detail elsewhere,[9,11] and here we restate the salient features. The governing equation for flow in a three-dimensional body (see Fig. 1) with porosity, ε, is obtained from the continuity equation in terms of the molar gas density, ρ, and gas velocity, u_i ($i = x, y,$ or z), in each direction:

$$-\left[\frac{\partial}{\partial x}(\rho u_x) + \frac{\partial}{\partial y}(\rho u_y) + \frac{\partial}{\partial z}(\rho u_z)\right] + \frac{r'}{M} = \frac{\partial(\rho\varepsilon)}{\partial t} \tag{1}$$

The rate of binder degradation is denoted by r', and M is the molecular weight of the decomposition products. The gas velocities in Eq. (1) can be obtained from Darcy's law:

$$u_i = -\left(\frac{\kappa_i}{\mu}\right)\frac{\partial P}{\partial i} \tag{2}$$

where μ is the viscosity. The permeability in each direction, κ_i, which can be obtained from the Kozeny-Carmen equation, is

$$\kappa_i = \frac{\varepsilon^3}{k_i(1-\varepsilon)^2 S^2} \tag{3}$$

where k_i is the Kozeny-Carmen parameter and S is the surface area per unit volume. If the pore size is sufficiently small so that slip flow prevails,[15–18] then Eq. (2) can be corrected to account for this. At low pressures, ρ is related to the pressure by the ideal gas law as

$$P = \rho RT \tag{4}$$

Combination of Eqs. (1), (2), and (4) leads to

$$\frac{\partial}{\partial x}\left(\rho\left(\frac{\kappa_x}{\mu}\right)\frac{\partial(\rho RT)}{\partial x}\right) + \frac{\partial}{\partial y}\left(\rho\left(\frac{\kappa_y}{\mu}\right)\frac{\partial(\rho RT)}{\partial y}\right) + \frac{\partial}{\partial z}\left(\rho\left(\frac{\kappa_z}{\mu}\right)\frac{\partial(\rho RT)}{\partial z}\right) + \frac{r'}{M} = \frac{\partial(\rho\varepsilon)}{\partial t} \tag{5}$$

J. A. Lewis—contributing editor

Manuscript No. 186492. Received December 12, 2002; approved July 16, 2003.

*Member, American Ceramic Society.

†Author to whom correspondence should be addressed. e-mail: LombardoS@missouri.edu.

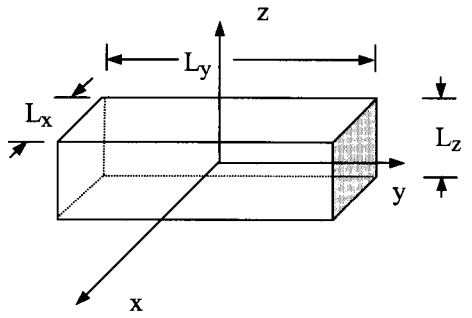

Fig. 1. Schematic of the green body defining the coordinate system and the length scales of the body.

This nonlinear partial differential equation, which is the governing equation for describing flow in porous media when a source term is present, requires numerical methods to obtain a solution. We have shown, however, that an analytical solution to Eq. (5) can be obtained which very accurately describes the pressure distribution in green bodies during the heating cycle.[9,11] To obtain the analytical solution, we invoke the pseudo-steady state and the following commonly used assumptions:[5,8,13] (1) the temperature distribution in the body is uniform because of the slow heating rates and multiple hold periods used in binder removal cycles; (2) the viscosity of the gas is constant during the heating cycle; and (3) the dimensional changes of the green body during binder removal are small and thus do not influence the pressure distribution.

To proceed further, we define dimensionless "stretched" distances and gas density, each denoted by an overbar, as

$$\bar{x} = \frac{2x}{L_x} \tag{6a}$$

$$\bar{y} = \sqrt{\frac{\kappa_x}{\kappa_y}}\left(\frac{2y}{L_x}\right) \tag{6b}$$

$$\bar{z} = \sqrt{\frac{\kappa_x}{\kappa_z}}\left(\frac{2z}{L_x}\right) \tag{6c}$$

$$\bar{\rho} = \frac{\rho}{\rho_0} \tag{7}$$

We next invoke the pseudo-steady-state assumption and use the transformation $\phi = \bar{\rho}^2$, which leads to

$$\frac{\partial^2\phi}{\partial\bar{x}^2} + \frac{\partial^2\phi}{\partial\bar{y}^2} + \frac{\partial^2\phi}{\partial\bar{z}^2} + C = 0 \tag{8}$$

with

$$C = \frac{L_x^2}{2\rho_0^2\kappa_x}\left(\frac{\mu}{RT}\right)\left(\frac{r'}{M}\right) \tag{9}$$

The initial condition for Eqs. (5) and (8) is $\bar{\rho} = 1$ at $t = 0$ everywhere in the body, and the boundary condition at the dimensionless "stretched" edges of the body

$$L = 1 \tag{10a}$$

$$W = \sqrt{\frac{\kappa_x}{\kappa_y}}\left(\frac{L_y}{L_x}\right) \tag{10b}$$

$$H = \sqrt{\frac{\kappa_x}{\kappa_z}}\left(\frac{L_z}{L_x}\right) \tag{10c}$$

is

$$\bar{\rho} = \frac{T_0}{T} \tag{11}$$

By recognizing that Eq. (8) is Poisson's equation, we can derive an analytical solution as[9,11]

$$\phi = \left(\frac{T_0}{T}\right)^2 + \sum_{i=1,3,5,\ldots}\sum_{j=1,3,5,\ldots}\sum_{k=1,3,5,\ldots} A_{ijk}\cos\left(\frac{i\pi\bar{x}}{2}\right)\cos\left(\frac{j\pi\bar{y}}{2W}\right)\cos\left(\frac{k\pi\bar{z}}{2H}\right) \tag{12}$$

where

$$A_{ijk} = 8C\left(\frac{2}{\pi}\right)^5\left(\frac{1}{ijk\left[i^2 + \left(\frac{j}{W}\right)^2 + \left(\frac{k}{H}\right)^2\right]}\right)(-1)^{(i+j+k-3)/2} \tag{13}$$

Once $\bar{\rho}$ has been determined, the pressure anywhere within the body can be obtained from

$$\frac{P}{P_0} = \bar{\rho}\,\frac{T}{T_0} \tag{14}$$

To complete the model description, we specify the rate of binder decomposition, r', with activation energy, E, and preexponential factor, A, as

$$r' = -\left(\frac{d(\rho_b\varepsilon_b)}{dt}\right) = A\exp\left[-\left(\frac{E}{RT}\right)\right]\rho_b\varepsilon_b/\varepsilon_{b,0} \tag{15}$$

where ρ_b is the density of the binder and $\varepsilon_{b,0}$ is the initial volume fraction of binder. The volume fraction of binder, ε_b, is related to the volume fractions of the porosity, ε, and the solid, ε_s, as

$$\varepsilon = 1 - \varepsilon_s - \varepsilon_b \tag{16}$$

As the reaction proceeds and binder decomposes to gas-phase products, the evolution of the volume fraction of binder is given by

$$\varepsilon_b = \varepsilon_{b,0} - \int_0^t \frac{r'}{\rho_b}\,dt \tag{17}$$

We have demonstrated previously that the analytical series solution given by Eq. (12) converges rapidly,[9,11] and thus the leading term solution can be used. This can be further simplified by considering the maximum pressure at the center of the body, $(P/P_0)_0$, as

$$\left(\frac{P}{P_0}\right)_0 \approx \left[1 + 0.8365\left(\frac{L_x^2}{2\rho_0^2\kappa_x}\right)\left(\frac{\mu}{R}\right)\left(\frac{r'}{M}\right)\left(\frac{T}{T_0^2}\right)\times\left(\frac{W^2H^2}{W^2H^2 + W^2 + H^2}\right)^{1/2}\right. \tag{18}$$

where C has been replaced by Eq. (9).

III. Results and Discussion

(1) Minimum Cycle Times for Binder Removal

Our earlier work[10] has shown that the normal stresses within green bodies during binder removal, as determined by finite element calculations, scale with increases in pressure within the body. We can thus use the pressure buildup, for which we have an analytical solution, to determine how the heating cycle should be varied during binder removal. To find the minimum cycle time, t^*, to remove the binder, we treat the reaction of binder volume fraction into degradation products as

$$\varepsilon_b \rightarrow \text{Products} \tag{19}$$

where the rate, $r(\varepsilon_b,T) = r'/\rho_b$, can be expressed as

$$\frac{d\varepsilon_b}{dt} = -r(\varepsilon_b, T) \tag{20}$$

We can formally integrate Eq. (20) from $t = 0$, $\varepsilon_b = \varepsilon_{b,0}$ at $T = T_0$ to $t = t^*$, $\varepsilon_b = 0$ at $T = T^*$ and solve for t^* as

$$t^* = \int_0^{\varepsilon_{b,0}} \frac{d\varepsilon_b}{r(\varepsilon_b, T)} \tag{21}$$

The heating profile $T(t)$ which determines $r(\varepsilon_b,T)$ so that t^* is a minimum is a problem of variational calculus,[19] because $T(t)$ is not known a priori. The function $r(\varepsilon_b,T)$ corresponding to the minimum time in Eq. (21) is the trivial solution of operating at the highest possible temperature where the decomposition rate is high. When a threshold pressure ratio, P_t, exists, however, that cannot be exceeded during the heating cycle, the integral in Eq. (21) must be minimized while simultaneously satisfying the constraint

$$(P/P_0)_0 = P_t \tag{22}$$

at $t = 0$ and for all times. This can be accomplished by solving the nonlinear Eq. (18) for new values of T as a function of t. This algorithm thus corresponds to varying the heating cycle in such a manner so that the pressure in the center of the body always corresponds to the threshold value, and thus failure does not occur.

Minimum times t^* were determined for a fixed body size and different threshold pressures with the parameters in Table I. Figure 2 indicates that, for a given threshold pressure, the heating cycle corresponding to the minimum time arises from a continuous increase in the temperature with time, i.e., a continuous increase in the heating rate with time. The form of the heating profiles in Fig. 2 can be explained by noting that in the early stage of binder removal when the porosity is low, the heating rates are low as well, and as binder is removed, the temperature can be increased more rapidly as the pore space becomes open and flow of decomposition products out of the body is facilitated. For larger values of the threshold pressure, which implies a stronger green body, the temperature can be increased very quickly and thus lead to shorter cycle times. For low values of the threshold pressure only slightly above ambient, which may correspond to avoiding bubble or blister formation, the cycle times can become very long.

Figure 3 shows for the case of $P_t = 1.1$ how other quantities of interest are varying during the heating cycle determined by variational calculus. In the early part of the binder removal cycle, the temperature must be increased gradually to satisfy the constraint of the threshold pressure. As the temperature is increased and the volume fraction of binder decreases, the permeability increases. The increase in the reaction rate, which depends on the volume fraction of binder, arises because the exponential effect of temperature more than compensates for the consumption of binder. The combined effect of these changes offsets each other, however, to maintain a nearly constant value of the quantity C.

Table I. Values of the Parameters Used in the Simulations

Symbol and description	Value and units
A, preexponential factor	8.5×10^{15} s^{-1}
E, activation energy	151 kJ/mol
T_0, initial temperature	300 K
P_0, initial ambient pressure	0.1 MPa
ε_S, solids fraction	0.5
$\varepsilon_{b,0}$, initial binder fraction	0.30
ρ_b, binder density	1000 kg/m^3
M, average molecular weight of gas products	0.044 kg/mol
μ, gas viscosity	0.025×10^{-3} Pa·s
S, surface area per unit volume	6×10^6 m^{-1}
k_i, Kozeny-Carman parameter	5

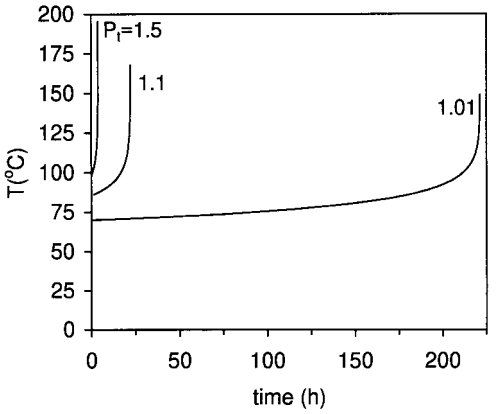

Fig. 2. Temperature profiles with time determined by variational calculus as a function of threshold pressure for a body of $L_x = 4$ cm, $L_y = 3$ cm, and $L_z = 2$ cm.

For the specific case of $L_x = 4$ cm, $L_y = 3$ cm, and $L_z = 2$ cm and a threshold pressure ratio of $P_t = 1.1$, the minimum cycle time is 22 h. When the same body is held at a constant soak temperature of 85.5°C, where $P_t = 1.1$ at $t = 0$, the cycle time is 186 h. If the same body is heated at the initial heating rate $\beta_0 = 10^{-4}$ °C/s (the tangent to the curve in Fig. 2 as $t \rightarrow 0$), the cycle time is 64 h. These comparisons illustrate the strong effect that increasing the temperature in a continuous fashion can have on the duration of the binder removal cycle. Because many temperature controllers are based on using a sequence of ramps and holds, the heating cycles in Fig. 2 for the minimum cycle times can be approximated as piecewise linear.

Other values of t^* are contained in Table II for different conditions. For $L_x = 4$ cm, $L_y = 3$ cm, and $L_z = 2$ cm with equal permeability in all directions, the cycle length increases as the threshold pressure decreases. For the same body size with a fixed $P_t = 1.1$, decreasing the permeability in one direction leads to an increase in the duration of the binder removal cycle. The cycle length is longest when the permeability is smaller in the shortest direction, because this resistance then has dominant control on gas evolution from the body. The third set of results in Table II is for isotropic permeability and a fixed $P_t = 1.1$. As all the body dimensions are doubled, and the component volume thus increases by a factor of 8, the minimum cycle time increases by a factor of ~4.

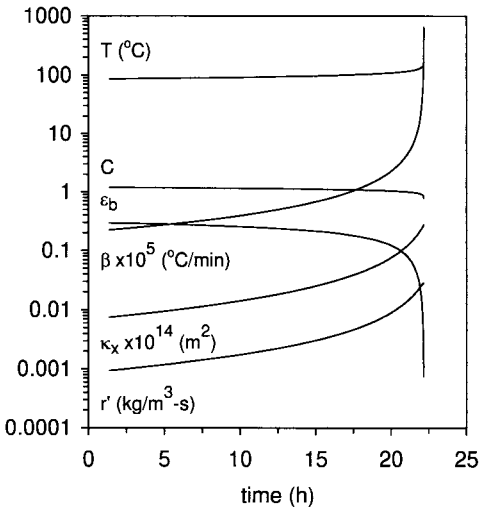

Fig. 3. Temperature, heating rate, permeability, volume fraction of binder, reaction rate, and C as a function of time determined by variational calculus for $P_t = 1.1$ for a body of $L_x = 4$ cm, $L_y = 3$ cm, and $L_z = 2$ cm.

Table II. Dependence of Minimum Cycle Time on Body Dimensions, Threshold Pressure, and Permeability

L_x (cm)	L_y (cm)	L_z (cm)	P_t	t^* (h)	Permeability
4	3	2	1.5	3.9	$\kappa_x = \kappa_y = \kappa_z$
4	3	2	1.1	22	$\kappa_x = \kappa_y = \kappa_z$
4	3	2	1.01	221	$\kappa_x = \kappa_y = \kappa_z$
4	3	2	1.1	47	$\kappa_x = \kappa_y$, $\kappa_z = \kappa_x/10$
4	3	2	1.1	29	$\kappa_x = \kappa_z$, $\kappa_y = \kappa_x/10$
4	3	2	1.1	25	$\kappa_y = \kappa_z$, $\kappa_x = \kappa_y/10$
2	1.5	1	1.1	5.7	$\kappa_x = \kappa_y = \kappa_z$
4	3	2	1.1	22	$\kappa_x = \kappa_y = \kappa_z$
8	6	4	1.1	86	$\kappa_x = \kappa_y = \kappa_z$

Finally, we note that when the threshold pressure is large, the cycle times for binder removal are so short that gradients in temperature, and thus binder distribution, may arise within the body. This more complicated case can then be evaluated by using the full set of equations for the coupled heat and mass transfer[4–8,13] in conjunction with equations of the form of Eqs. (21) and (22).

(2) Optimization of Body Geometry

We first address the topic of the coupling between length scales and permeabilities and how their combined effect influences the buildup of pressure within a porous green body. We treat this case by analyzing how the specification of body geometry can mitigate the buildup of pressure within a body. Although this is not feasible for many applications, where other design considerations influence the component shape, multilayer ceramic capacitors (MLCs) often are designed specifically to deliver a fixed amount of charge storage and thus can have different shapes to satisfy this requirement. For a fixed layer thickness, the charge storage is proportional to the number of layers and hence to the volume of the capacitor. We are thus interested in knowing how the geometry of the capacitor influences the buildup of pressure within the component. We start with highly symmetric shapes and then relax this requirement to treat more asymmetric geometries.

(A) Bodies of Fixed-Volume Cubes: The first case is for the pressure buildup when the volume of the cubic body, V, is fixed and given as $V = L_x L_y L_z$. With this relationship, Eq. (18) can be rewritten in terms of the volume as

$$\left(\frac{P}{P_0}\right)_0 = \left[1 + 0.8365\lambda\left(\frac{\kappa_x}{\sqrt{\kappa_y\kappa_z}}V\right)^{2/3}\left(\frac{W^{4/3}H^{4/3}}{W^2H^2 + W^2 + H^2}\right)\right]^{1/2} \quad (23)$$

where $\lambda = \mu r' T/(2\rho_0^2\kappa_x RT_0^2 M)$. The maximum in $(P/P_0)_0$ given by Eq. (23) occurs at $L = W = H = 1$. Thus, for a body of fixed volume and equal permeability in all directions, the maximum pressure buildup in the center of the body occurs when the body is a cube. If the permeability in the body is anisotropic, then the maximum in pressure still occurs for the highly symmetric shape $L = W = H = 1$, which now corresponds to equivalent "stretched" dimensions but unequal real dimensions, as given by Eqs. (6) and (10).

(B) Bodies of Fixed-Volume Square Parallelepipeds: As the volume is held fixed for isotropic permeability with $L = W = 1$ but H is allowed to vary, the geometry now corresponds to that of a square parallelepiped. The dependence of $(P/P_0)_0$ on H for isotropic permeability in the body is shown in Fig. 4(a), where a maximum in $(P/P_0)_0$ is observed at $H = 1$, which is the geometry corresponding to a cube. For anisotropic permeability given by $\kappa_x = \kappa_y$ and $\kappa_z = \kappa_x/10$, the maximum in $(P/P_0)_0$ still occurs at $H = 1$, but the magnitude is now 50% larger.

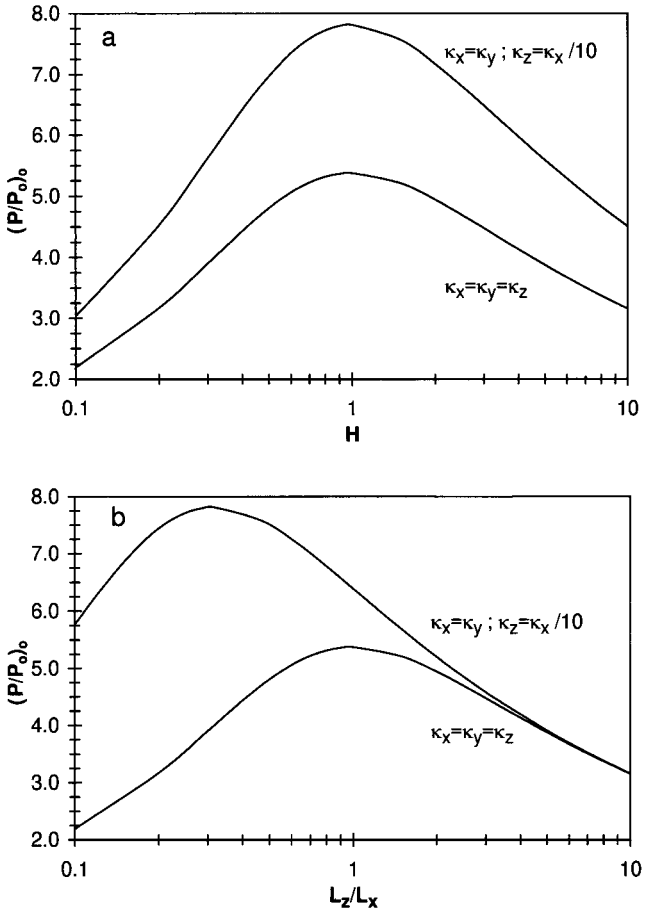

Fig. 4. Dependence of $(P/P_0)_0$ with (a) H and (b) L_z/L_x for $W = 1$ for isotopic and anisotropic permeabilities for a constant body volume.

A subtle point regarding the maximum in $(P/P_0)_0$ can be observed by replotting the data in Fig. 4(a) versus L_z/L_x as in Fig. 4(b). When the permeabilities are equal, the maximum in $(P/P_0)_0$ occurs at $L_z = L_x$. When the permeabilities are unequal, the maximum in $(P/P_0)_0$ occurs at a lower aspect ratio. The aspect ratio of a square parallelepiped corresponding to the maximum in $(P/P_0)_0$ can be established by differentiating Eq. (23) under the constraint of constant volume which leads to $H = 1$ or

$$\frac{L_z}{L_x} = \sqrt{\frac{\kappa_z}{\kappa_x}} \quad (24)$$

For the conditions of $\kappa_z = \kappa_x/10$ in Fig. 4(b), the maximum in $(P/P_0)_0$ occurs at $L_z/L_x = 0.32$.

The occurrence of a maximum in $(P/P_0)_0$ in Fig. 4(b) for isotropic permeability in square-parallelepiped bodies of fixed volume can be rationalized in the following manner. For very small L_z, the distance in this direction is so short that flow to the exterior of the body keeps the pressure buildup small. As L_z increases relative to L_x, the pressure buildup increases as all pathways out of the body become more equal until a maximum is achieved at the geometry corresponding to a cube. Further increases in L_z/L_x now lead to shorter pathways out of the body in the x- and y-directions, and the buildup of pressure is thus smaller.

For the case in Fig. 4(b) where the permeability in the z-direction is lower as compared with the x- and y-directions, the pressure in the body increases as a consequence of the larger overall resistance to flow. The coupling between κ_z and L_z, however, combines to shift the maximum pressure increase to the aspect ratio of $L_z/L_x = 0.32$. For smaller values of this ratio, flow

in the *z*-direction is facilitated, and the increase in pressure is lower. For values of L_z much larger than $0.32L_x$, the resistances in the *x*- and *y*-directions become controlling. In fact, as seen in Fig. 4(b) for sufficiently large L_z/L_x, $(P/P_0)_0$ approaches the same asymptotical behavior as was observed for equal permeabilities in all directions; in other words, the resistance in the *z*-direction only negligibly influences $(P/P_0)_0$. This behavior is analogous to electrical resistors in parallel, in which, for widely disparate values, the lowest resistance becomes the controlling factor.

(C) Bodies of Fixed-Volume Rectangular Parallelepipeds: The cases treated above correspond, for isotropic permeability, to bodies of square-parallelepiped geometry. The last case examined here is for rectangular parallelepipeds, when all dimensions may be unequal. When the height to length ratio of the body L_z/L_x is held fixed for a prescribed volume of capacitor, the maximum in $(P/P_0)_0$ depends on the value of H, as is indicated in Fig. 5. As H increases, the maximum in $(P/P_0)_0$ shifts to higher values of W. For a given value of H, the value of W corresponding to the maximum $(P/P_0)_0$ is given by

$$W = \sqrt{\frac{2H^2}{H^2 + 1}} \tag{25}$$

The lower pressure ratios arising for high-aspect-ratio bodies can again be rationalized by noting that as one dimension becomes small, flow out of the body in this direction is facilitated and the buildup of pressure is thus mitigated.

When only the height of the body is fixed and the ratio of the two side lengths L_x and L_y are allowed to vary for a constant volume of capacitor, the buildup of pressure within the body can be treated as well. For this case, Fig. 6 indicates that the maximum in $(P/P_0)_0$ occurs at $W = L_y/L_x = 1$. For equal permeability within the body, this corresponds to a cube, where all pathways out of the body are equivalent. For less symmetric bodies, shorter pathways will be present that will facilitate flow out of the body, thereby resulting in lower pressure. Fabricating capacitors at higher aspect ratios is thus one means of mitigating the buildup of pressure within MLCs. In the experiments of Liau *et al.*,[13] rectangular MLC parallelepipeds survived binder removal at a higher yield than was observed for square MLC parallelepipeds for the same volume of body.

For the case of lower permeability in the *z*-direction as given by $\kappa_x = \kappa_y$ and $\kappa_z = 0.1\kappa_x$, the maximum in pressure in Fig. 6 is again observed at $L_x = L_y$, but the absolute value of $(P/P_0)_0$ is now twice as large and the variation in $(P/P_0)_0$ with L_y/L_x is much more pronounced. Whereas $(P/P_0)_0$ varies by 15% for an aspect ratio of $L_y/L_x = 9$ versus $L_y/L_x = 1$ for equal permeabilities, $(P/P_0)_0$ varies by 50% over the same range of aspect ratios for a body with anisotropic permeability. The results in Fig. 6 indicate that $(P/P_0)_0$ is symmetric about variations in L_y/L_x for a fixed volume of capacitor, regardless of the value of the permeability in the *z*-direction. This arises because the permeability in the *z*-direction is independent of the dimensions L_x and L_y, and thus no direct coupling occurs between the length scales L_x and L_y and the permeability κ_z.

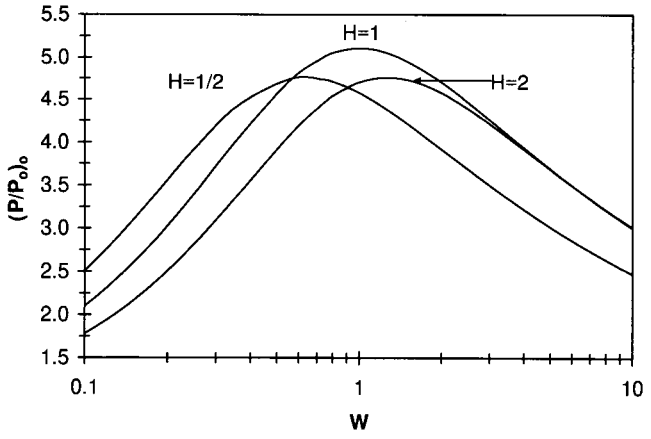

Fig. 5. Dependence of $(P/P_0)_0$ with W for different values of H for a constant body volume.

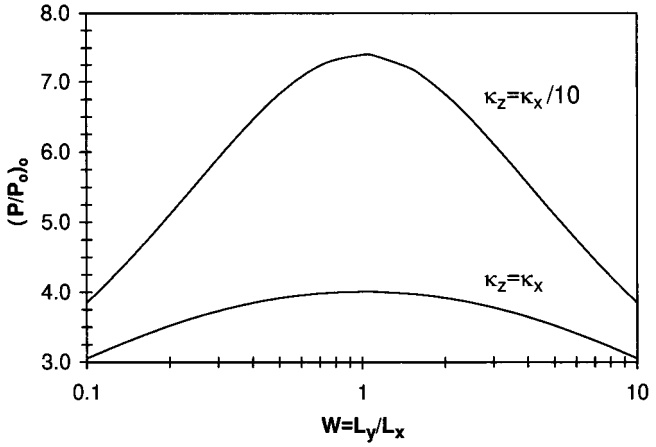

Fig. 6. Dependence of $(P/P_0)_0$ with $W = L_y/L_x$ for isotopic and anisotropic permeabilities for a constant body volume.

IV. Conclusions

A previously developed three-dimensional model for describing flow in porous media when a source term is present has been applied to two aspects of optimization for the binder removal process. For determining the minimum time for the binder removal cycle, a computational algorithm based on variational calculus has been developed. This optimization strategy indicates that, for a fixed threshold pressure within the body, the minimum cycle time for binder removal arises from a continuous increase in the heating rate with time. This approach can lead to very significant reductions in the cycle length as compared with using constant-temperature hold periods or linear heating rates.

For bodies of fixed volume, the model can be used to determine what type of body geometry mitigates the buildup of pressure within the component. The model can be used to treat both isotropic and anisotropic permeability within the component. An important outcome of this analysis is that the coupling of dimension and permeability has been captured in terms of "stretched" dimensionless quantities, which allows the problem to be rationalized in terms of resistances in parallel.

References

[1]R. M. German, "Theory of Thermal Debinding," *Int. J. Powder Metall.*, **23**, 237–45 (1987).

[2]J. A. Lewis, "Binder Removal From Ceramics," *Annu. Rev. Mater. Sci.*, **27**, 147–73 (1997).

[3]P. Calvert and M. Cima, "Theoretical Models for Binder Burnout," *J. Am. Ceram. Soc.*, **73** [3] 575–79 (1990).

[4]G. Y. Stangle and I. A. Aksay, "Simultaneous Momentum, Heat and Mass Transfer with Chemical Reaction in a Disordered Porous Medium: Application to Binder Removal from a Ceramic Green Body," *Chem. Eng. Sci.*, **45**, 1719–31 (1990).

[5]D.-S. Tsai, "Pressure Buildup and Internal Stresses during Binder Burnout: Numerical Analysis," *AIChE J.*, **37**, 547–54 (1991).

[6]S. A. Matar, M. J. Edirisinghe, J. R. G. Evans, and E. H. Twizell, "Effect of Porosity Development on the Removal of Organic Vehicle from Ceramic or Metal Moldings," *J. Mater. Res.*, **8**, 617–25 (1993).

[7]J. H. Song, M. J. Edirisinghe, J. R. G. Evans, and E. H. Twizell, "Modeling the Effect of Gas Transport on the Formation of Defects during Thermolysis of Powder Moldings," *J. Mater. Res.*, **11**, 830–40 (1996).

[8]A. C. West and S. J. Lombardo, "The Role of Thermal and Transport Properties on the Binder Burnout of Injection Molded Ceramic Components," *Chem. Eng. J.*, **71**, 243–52 (1998).

[9]S. J. Lombardo and Z. C. Feng, "Pressure Distribution during Binder Burnout in Three-Dimensional Porous Ceramic Bodies with Anisotropic Permeability," *J. Mater. Res.*, **17**, 1434–40 (2002).

[10]Z. C. Feng, B. He, and S. J. Lombardo, "Stress Distribution in Porous Ceramic Bodies during Binder Burnout," *J. Appl. Mech.*, **69**, 497–501 (2002).

[11]K. Feng and S. J. Lombardo, "Modeling of the Pressure Distribution in Three-Dimensional Porous Green Bodies during Binder Removal," *J. Am. Ceram. Soc.*, **86** [2] 234–40 (2003).

[12]R. V. Shende and S. J. Lombardo, "Determination of Binder Decomposition Kinetics for Specifying Heating Parameters in Binder Burnout Cycles," *J. Am. Ceram. Soc.*, **85** [4] 780–86 (2002).

[13]L. C.-K. Liau, B. Peters, D. S. Krueger, A. Gordon, D. S. Viswanath, and S. J. Lombardo, "Role of Length Scale on Pressure Increase and Yield of Poly(vinyl butyral)–Barium Titanate–Platinum Multilayer Ceramic Capacitors during Binder Burnout," *J. Am. Ceram. Soc.*, **83** [11] 2645–53 (2000).

[14]B. Peters and S. J. Lombardo, "Optimization of Multi-Layer Ceramic Capacitor Geometry for Maximum Yield during Binder Burnout," *J. Mater. Sci.: Mater. Electron.*, **12**, 403–409 (2001).

[15]L. J. Klinkenberg, "The Permeability of Porous Media to Liquids and Gases," *Drill. Prod. Pract. API*, 200–13 (1941).

[16]G. P. Brown, A. DiNardo, G. K. Cheng, and T. K. Sherwood, "The Flow of Gases in Pipes at Low Pressures," *J. Appl. Phys.*, **17**, 802–13 (1946).

[17]N. Wakao, S. Otani, and J. M. Smith, "Significance of Pressure Gradients in Porous Materials: Part I. Diffusion and Flow in Fine Capillaries," *AIChE J.*, **11**, 435–39 (1965).

[18]S. Otani, N. Wakao, and J. M. Smith, "Significance of Pressure Gradients in Porous Materials: Part II. Diffusion and Flow in Porous Catalysts," *AIChE J.*, **11**, 439–45 (1965).

[19]M. M. Denn, *Optimization by Variational Methods.* McGraw-Hill, New York, 1969. □